COBEM 2023 27TH INTERNATIONAL CONGRESS OF MECHANICAL ENGINEERING

ABCM Brazilian Society of Mechanical Sciences and Engineering
27th ABCM International Congress of Mechanical Engineering
December 04-08, 2023, Florianópolis-SC, Brazil

COB-2023-1713
INVESTIGATION OF RESONANT SHUNT CIRCUIT CONNECTED TO PIEZOELECTRIC PADS FOR LOW-FREQUENCY TUNING

Braion Barbosa de Moura[1]
Daniely Amorim das Neves[1]
Edgar Jhonny Amaya Simeon[2]
Marcela Rodrigues Machado[1]
[1] Department of Mechanical Engineering, University of Brasília, 70910-900, Brasília, Brazil.
[2] Department of Electrical Engineering, University of Brasília, 70910-900, Brasília, Brazil.
braionbarbosa@gmail.com

Abstract. *This article addresses an electromechanical investigation of a piezoelectric path subject to vibrations that is connected in series to a resistive-inductive type shunt circuit. The main idea of this investigation is to predict the ideal values of the electronic components so that the shunt circuit is tuned to a low frequency, approximately below 20 Hz. In this sense, it is necessary to use a synthetic inductance to guarantee non-interference in the electromagnetic radiation field of nearby components and also avoid using coils with large volumes. Furthermore, the development of a configuration of a piezoelectric path connected to a resonant shunt circuit tuned at low frequency with almost zero tuning error margins is a tool with enormous potential to promote passive vibration control in various applications. Therefore, this work explores an electrical simulation based on the characterization of a real signal from piezoelectric paths to compare three circuits that generate a synthetic inductance, they are: Antoniou; Riodan; and Gyrator. For this, four combinations of resistive component values are created to try to elucidate whether the high resistance value implies any improvement in tuning. Finally, the tuning variation suffered by the tolerance of the components that form all shunt circuits analyzed is also analyzed.*

Keywords: *Vibration control, Passive shunt circuit, Synthetic inductance*

1. Introduction

The use of piezoelectric materials applied for vibration control and health monitoring is a study relevant and frequent in mechanical engineering, (Liu and Wang, 2023; Mahapatra *et al.*, 2021; Wang *et al.*, 2023). Due to their ability to convert electric energy into mechanical energy and vice versa, called the direct and inverse piezoelectric effect (Akedo *et al.*, 2017). In the direct piezoelectric effect, piezoelectric materials can be used as sensing devices to detect parameters measuring electrical voltages when combined with additional circuitry (Pan and Guan, 2022). In the inverse effect, piezoelectric materials can be used as actuators to control mechanical vibrations, since an electrical voltage causes a mechanical deformation (Molter *et al.*, 2019; Abdalla *et al.*, 2005). Thus, piezoelectric materials have several advantages for use in vibration control, including easy installation and maintenance, fast response, resistance to electromagnetic interference, and excellent electromechanical coupling properties, which make them suitable for noise control, vibration control, the transmission of performance and energy capture, among other applications.

The approaches to control vibrations using piezoelectric materials, there are active control, passive control, and hybrid control (Rui *et al.*, 2023). In active vibration control, piezoelectric materials are used as actuators and sensors, in which an external force is applied to the piezoelectric material to generate a mechanical deformation (Zhu *et al.*, 2018). This is a frequently used approach in many applications, however, its main disadvantages, besides the use of an external force, are the high complexity and low stability. In passive control, piezoelectric materials are used to change the system's stiffness or damping characteristics, to absorb and dissipate vibrational energy (He *et al.*, 2019). In this approach, it is not necessary to use external sources and piezoelectric materials as energy transducers and connect shunt circuits. Finally, hybrid control combines elements of both passive and active approaches. In passive damping devices, vibrational energy is converted into electrical energy using piezoelectric materials. A piezoelectric material can also be used as a feedback mechanism in an active control system to detect vibrations, thereby making it more efficient and adaptable (Rui *et al.*, 2023).

In passive control, piezoelectric materials are connected to electronic circuits called shunt which form a dissipation device that is designed to add damping to the mechanical system (Viana and Junior, 2006). Passive shunts provide very good vibration reduction in a specific mode or in multiple modes, depending on the damping device design and the frequency range to be reduced, but circuit elements must be closely tuned to the targeted frequencies. According Lesieutre (1998) there are four commonly used types of shunt circuits: restive, resonant, capacitive, and switched. But of all of

them, the resonant shunt circuit is the most recommended because it allows tuning to any frequency that you are interested in attenuating, and even the resolution of more than one frequency (Niederberger and Morari, 2006).

More recently, works like Yamada *et al.* (2010) showed some existing differences in the calculation of tuning for resistors and inductors of passive electrical circuits to control vibration. Antoniou's topography can be seen in several works, with different attunement configurations (Machado *et al.*, 2022, 2020; Yamada *et al.*, 2013). On top of this logic, Zambolini-Vicente *et al.* (2017) investigated the adoption of resistive and inductive parameters considering three distinct topographies of synthetic inductance, namely: Antoniou, Riodan and Gyrator.

In summary, some other works reported the use of synthetic inductor vibration control schemes, but little or no discussion of the different possibilities for such circuit inductors, as well as the performance mode or attenuation level are exposed. Therefore, this work proposes to demonstrate a simulated comparison of three synthetic inductances for low-frequency tuning, in order to verify if there are relations defined as a function of self resistance values for each of the synthetic inductances of Antoniou, Riodan and Gyrator.

1.1 Background

Some electrical arrangements with operational amplifiers can represent the operation of a simple inductive element. These arrangements are known as synthetic inductance's and have great electronic application because they require small physical spaces and do not generate an electromagnetic field. Among the synthetic inductance's most used for resonant tuning of signals, the inductance's of the Gyrator, Riodan and Antoniou circuits stand out, whose topography is illustrated in Fig. 1.

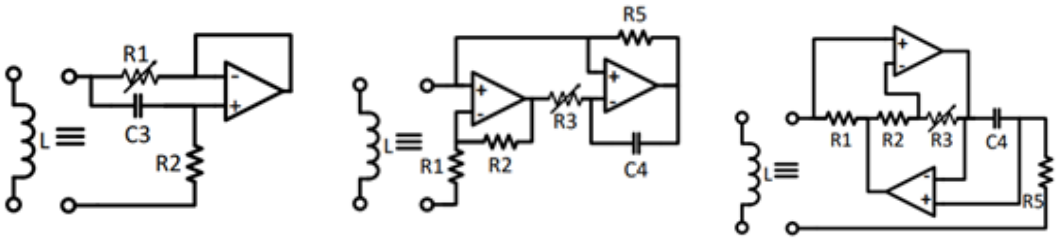

(a) (b) (c)

Figure 1: Topographic representation of synthetic inductance of the type: (a) Gyrator; (b) Riodan; (c) Antonio. FONTE: Zambolini-Vicente *et al.* (2017)

According Riodan (1967) and Antoniou (1969), the synthetic inductances of Antoniou and Riodan can be defined by the same calculation. Therefore, we can define the inductance of these circuits with:

$$L = \frac{R_1 R_3 R_4 C_1}{R_2}. \tag{1}$$

In the case of the Gyrator circuit, according Tellegen (1948), there is a different interpretation for calculating the inductance. The following expression is considered:

$$L = R_5 R_6 C_1. \tag{2}$$

When observing equations Eq. (1) and Eq. (2), it is noticed that the inductance will depend only on the resistive and capacitive elements. Therefore, the possibility of inductance adjustment with the change of these elements is evident.

In the case of connecting a piezoelectric pad with a resistor-inductor resonant shunt circuit in series, the topography of Fig. 2 may be considered.

Figure 2, it can be observed that the piezoelectric pad can be represented by the combination of a voltage source in series with a capacitor and the value of this source and the capacitor are inherent as geometric properties and materials of the type of pad placed in deformation. Given this relationship, Hagood stipulated a parameter to define the best value of resistance and inductance with:

$$R = \frac{\sqrt{2} K_{ij}}{C_P^T \omega_{nt} (1 + K_{ij}^2)}, \tag{3}$$

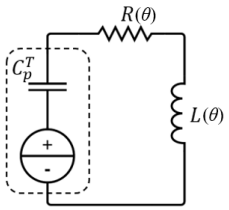

Figure 2: Representative topography of a piezoelectric chip connected to a series resistive-inductive circuit.

$$L = \frac{1}{C_P^T(1 + K_{ij}^2)\omega_{nt}} \tag{4}$$

were C_P^T is the piezoelectric capacitance, $K_{ij} = \sqrt{f_n^2 - f_s^2}/f_s$ is the generalized electromechanical coupling factor, R is the optimal resistor that precedes the inductance, L is the optimal inductance value and ω_{nt} is the tuning frequency given by:

$$\omega_{nt} = \sqrt{\frac{1}{C_P^T L}}. \tag{5}$$

Once the tuning frequency is defined considering the piezoelectric capacitance and the synthetic inductance, a mathematical relation of coupling of the structure element with the piezoelectric element connected to the circuit can be established (Machado *et al.*, 2022; Moura *et al.*, 2022; Machado *et al.*, 2020).

2. Results

Before simulating the piezoelectric pad connected to a circuit with synthetic inductance, it was first necessary to collect the typical electrical signal of a piezoelectric pad. For this purpose, 8 SMD07T05R412WL piezoelectric discs were periodically glued along an aluminum beam 1 meter long, 2 centimeters wide and 3 millimeters thick. At the end of this beam, an excitation was implemented through shake that oscillated a sweep function ranging from 3 to 1000 Hz. This experiment is shown in Figure 3.

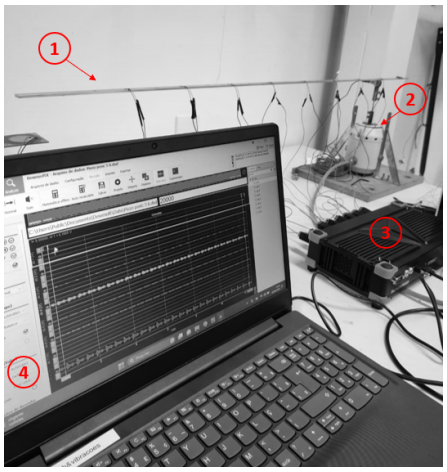

(a)

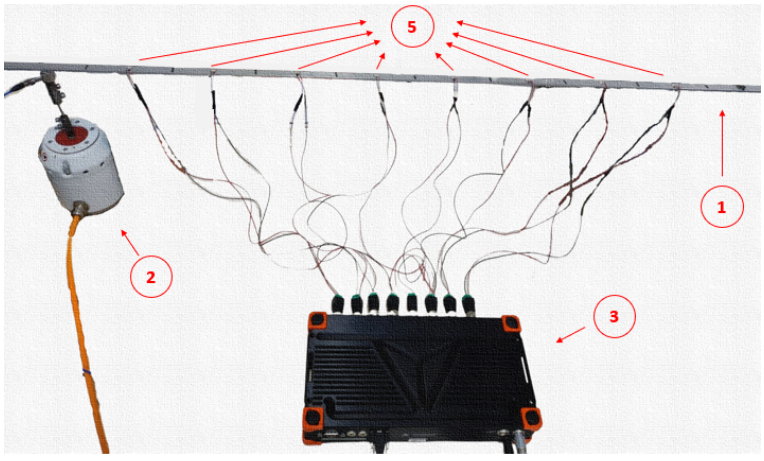

(b)

Figure 3: Setup of the experiment: (1) beam with eight piezoelectric, (2) shaker, (3) data acquisition system and (4) computer.

Figure 3 we have the setup of the experiment represented with: 1 indicates the aluminum beam where the piezoelectric pads are coupled; 2 indicates the shake that promotes excitation in the structure in free-free condition; 3 indicates the data acquisition hardware from the company DEWESoft®; and 4 indicating the software linked to the hardware that treats and plots the electrical data of each pad. It is suspected that these amplitudes may be located at 60 Hz due to interference from the public electrical signal in the hardware supply, but for the purpose of this study, this influence is disregarded.

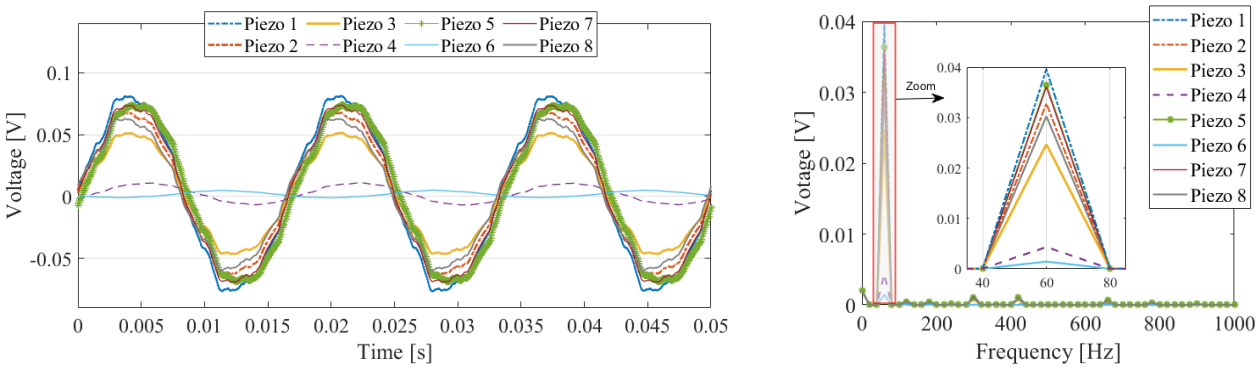

(a) (b)

Figure 4: Signal from each piezo as a function of (a) time and (b) frequency.

Figure 4a, one can observe the voltages as a function of the frequency of each piezoelectric pads. Basically, both signals present a larger peak located at the frequency of 60 Hz, but the amplitudes differ from piezo to piezo, having the following amplitude order: Piezo 1 (0.0395 dB); Piezo 5 (0.0363 dB); Piezo 7 (0.0360 dB); Piezo 2 (0.0327 dB); Piezo 8 (0.0302 dB); Piezo 3 (0.0246 dB); Piezo 4 (0.0043 dB); and Piezo 6 (0.0014 dB).

This piezoelectric voltage difference can be better observed as a function of time, as shown in Fig. 4b. While the highest amplitude of Piezo 1 is recorded around 83 mV, the highest amplitude of Piezo 6 is recorded at 5 mV . It is estimated that such difference is due to one or more of the following reasons: way of vibrating the beam favoring or disfavoring the deformation of a certain piezoelectric pads; factory defect; poor electrical conductivity; imperfect coupling; and positioning of the shake on the beam.

Given this scenario, we can approximate the collected data to an average piezoelectric signal with an amplitude of 0.07 mV and a frequency of 60 Hz. Therefore, we can connect this signal to the resonant shunt circuits with synthetic inductances, as shown in Fig. 5.

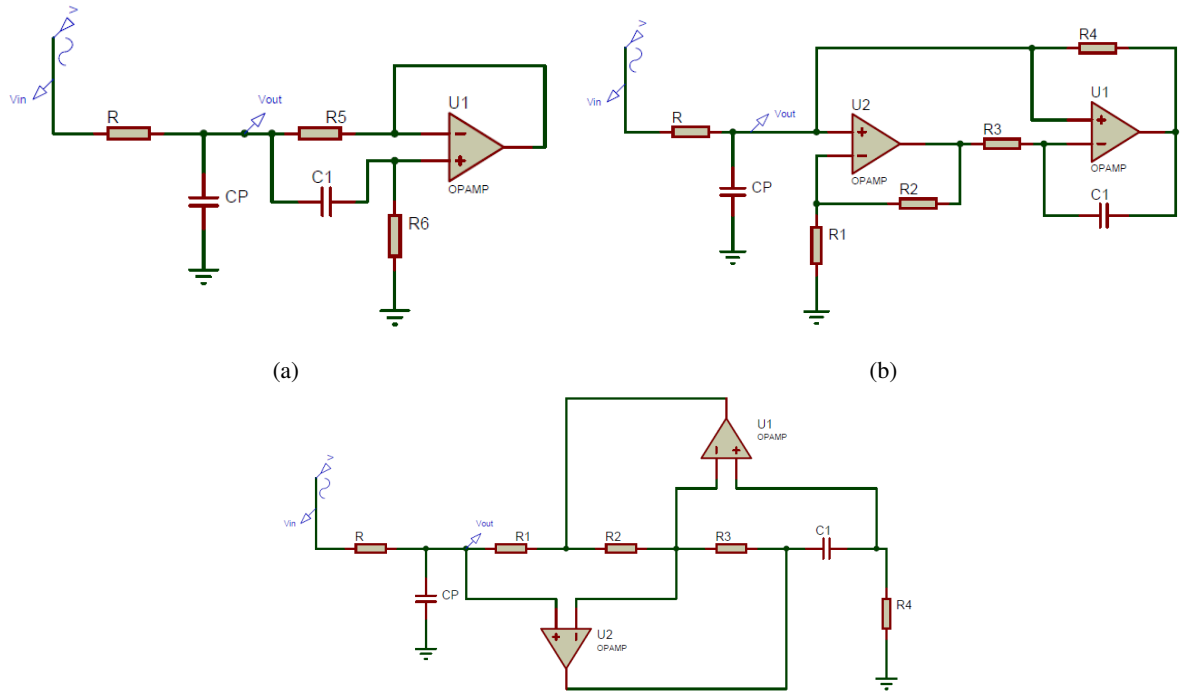

(a) (b)

(c)

Figure 5: Topographic representation of a piezoelectric pad connected to a resonant shunt circuit with synthetic inductance of the type: (a) Gyrator; (b) Riodan; (c) Antoniou.

All topographies shown in Figure 5 represent a connection of a piezoelectric chip with $C_P^T = 1.31nF$ connected to an RL circuit in series with general resistance $R = 200\Omega$ and inductance $L \approx 123KH$. All operational amplifiers used were

type 741 varying between +5 and -5 V. Capacitance $C_1 = 100\mu F$ was used in all synthetic inductance's and the values of the other components are illustrated in Tab. 1 for the Antoniou and Riodan circuit, and Tab. 2 for the Gyrator circuit.

Table 1: Values of electrical components adopted for circuits with synthetic inductance's by Antoniou and Riodan.

Experiment	$R_1[K\Omega]$	$R_2[K\Omega]$	$R_3[K\Omega]$	$R_4[K\Omega]$	**Frequency** ω_{sh}[Hz]
#1	4.3	0.033	2.2	4.3	12.5371
#2	8.2	0.510	9.1	8.2	12.7078
#3	33	24	27	33	12.5756
#4	330	22000	240	330	12.7706

Table 2: Values of electrical components adopted for circuits with synthetic inductance's by Gyrator.

Experiment	$R_5[K\Omega]$	$R_6[K\Omega]$	**Frequency** ω_{sh}[Hz]
#1	33	36	12.7706
#2	130	9.1	12.7976
#3	1000	1.2	12.7066
#4	22000	0.056	12.5405

Four combinations of resistive elements with commercial values were chosen to try to tune the same design frequency. Basically, the values were defined using Eq. (1) and Eq. (2), based on the best possible arrangement with small, medium and large resistance value. The main idea in choosing these values is justified by the possibility of interference in the piezoelectric output signal, since the amplitude has a relatively small value. Thus, by implementing the values of each case in Tab. 1 and 2 in the topographies shown in Fig. 5, we can demonstrate the Bode diagram in Fig. 6.

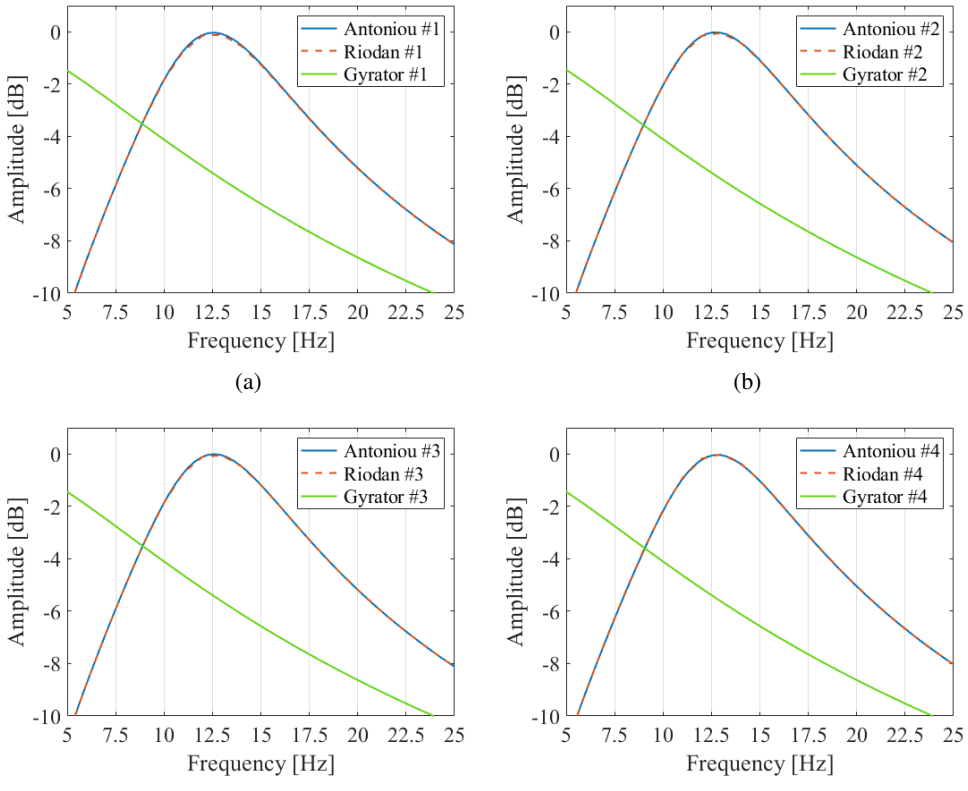

Figure 6: Comparison of piezoelectric connection magnitude in different series RL shunt circuits with synthetic L. (a) case #1; (b) case #2; (c) case #3; (d) case #4.

When comparing the magnitudes arising from different synthetic inductance's, a behavioral difference in the Gyrator inductance can be seen. Unlike what happens in Antoniou and Riodan, in Gyrator a peak located at the design frequency

is not noticeable. This fact can be observed in all four cases. Although the four cases seem to have a lot of behavioral similarity to each other, there is a difference in amplitude associated with each case and this can be seen in Fig. 7.

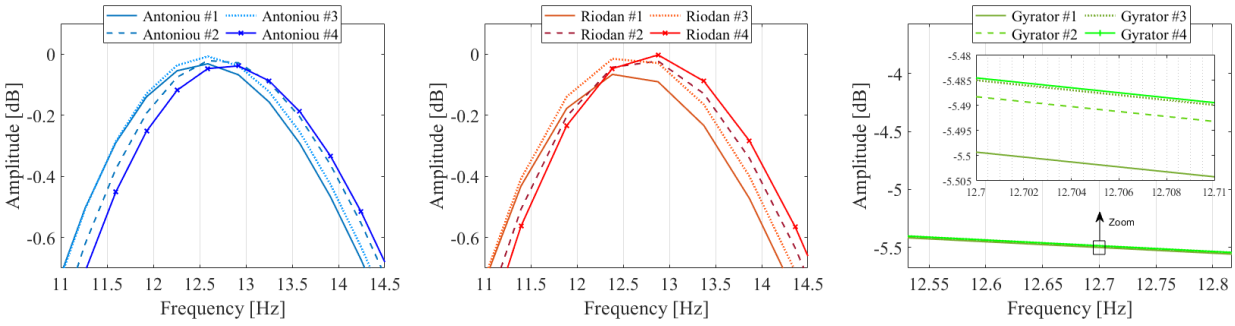

(a) (b) (c)

Figure 7: Comparison of piezoelectric connection magnitude in different series RL shunt circuits with synthetic L. (a) Antoniou; (b) Riodan; (c) Gyrator.

Although Antoniou and Riodan present the same component values, it is interesting to mention that cases #2 and #1 of Antoniou presented the highest and lowest amplitude, consequently. Cases #4 and #1 of Riodan had the highest and lowest amplitude, consequently. Another way to investigate these differences is through the analysis of stress as a function of time, as shown in Fig. 8.

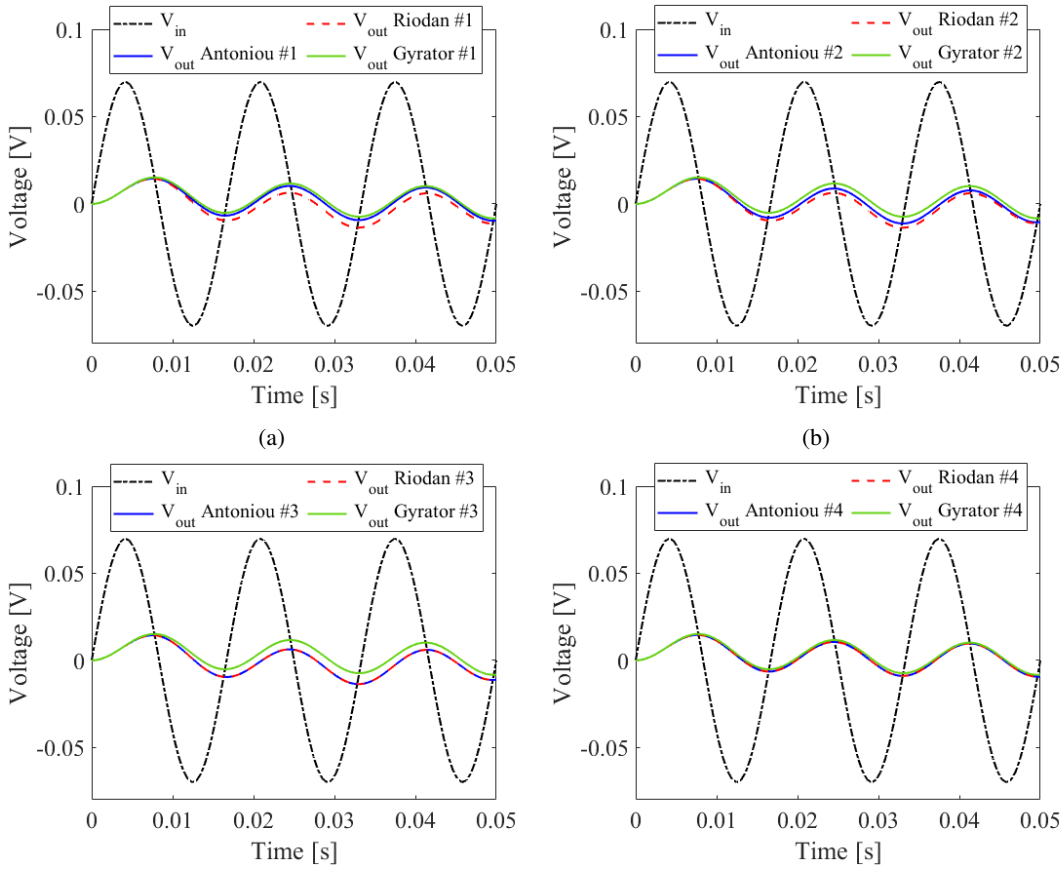

(a) (b) (c) (d)

Figure 8: Comparison of piezoelectric connection magnitude in different series RL shunt circuits with synthetic L. (a) case #1; (b) case #2; (c) case #3; (d) case #4.

Figure 8 it can be seen that attenuation is present in all cases and with all inductance's. However, there is a specific difference in amplitude associated with each case, for example: In case #1, Antoniou behavior is closer to Gyrator's; In

case #2, practically the three inductance's result in different behaviors; In case #3, Antoniou signal is similar to Riodan behavior; and in case #4 all inductance's have similar behavior.

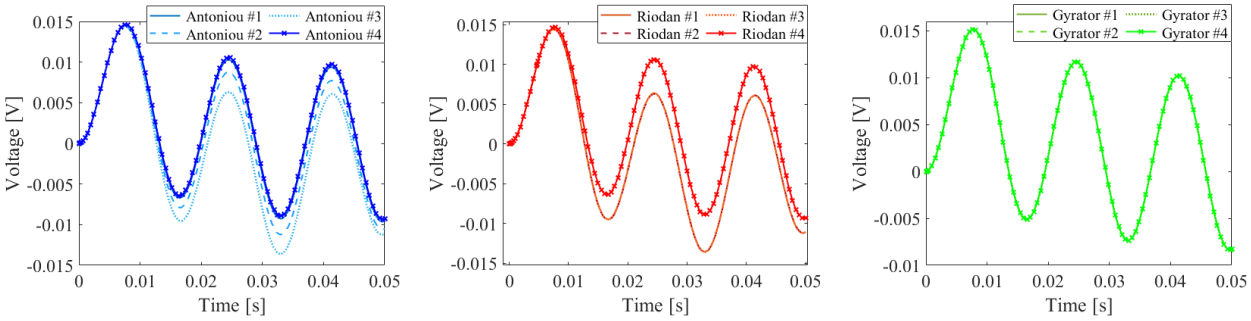

(a) (b) (c)

Figure 9: Comparison of piezoelectric connection voltage in different series RL shunt circuits with synthetic L. (a) Antoniou; (b) Riodan; (c) Gyrator.

Finally, when observing Fig. 9, we can see that both in the Antoniou and Riodan inductances, case #4 denotes a greater amplitude, but the smaller amplitude is that of case #3 for Antoniou and that of cases #2 and #3 for case Riodan. Regarding the Gyrator, all signals remain identical to each other regardless of the case.

In addition to analyzing all these conditions demonstrated above, it is interesting to analyze that these four tuning conditions explored may suffer a variation due to the tolerance rate of the electronic components, more specifically the resistors. Figure 10 demonstrates this variation for the Antoniou circuit cases.

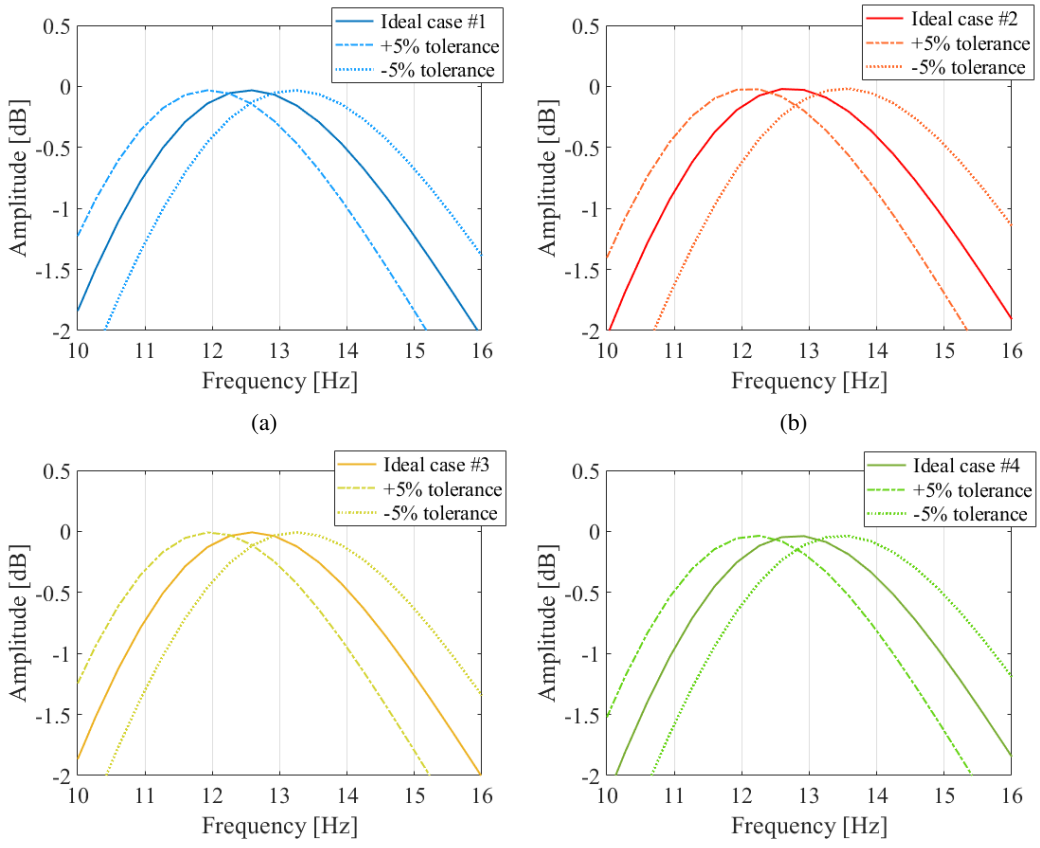

(a) (b) (c) (d)

Figure 10: Comparison of the magnitude of the piezoelectric connection in RL series shunt circuits with a 5% resistive tolerance variation, with the synthetic L originating from the Antoniou circuit. (a) case #1; (b) case #2; (c) case #3; (d) case #4.

Figure 10 it can be seen that the tuning undergoes a variation in both cases. Although the simulated elements have a

tolerance of 5%, onsidered one of the smallest for common components, a variation in frequency of approximately 0.8 Hz up and down is noticeable. This reinforces that a spot check must be carried out in each case where perfect tuning is to be guaranteed.

3. CONCLUSIONS

The conclusions of this work denote a specific interpretation that the synthetic impedances of Antoniou and Riodan were very similar both in the frequency aspect and in the temporal aspect, unlike the Gyrator that presented more similarity only in the temporal aspect. However, it can also be argued that the elaboration of inductances with low and high value resistive elements impacted little or almost no interference in the signal, since the amplitudes arising from each configuration are not very distant from each other. It can also be concluded that regardless of the resistance value used, the component tolerance of 5% exerts a considerable variation in the design frequency. In summary, it should be noted that to define the best synthetic impedance at low frequency it is recommended to carry out comparative vibrational attenuation experiments.

4. ACKNOWLEDGEMENTS

The author appreciate the supports from Fundação de Apoio a Pesquisa do Distrito Federal-FAPDF (under grant number 00193-00000766/2021-71).

5. REFERENCES

Abdalla, M., Frecker, M., Gürdal, Z., Johnson, T. and Lindner, D.K., 2005. "Design of a piezoelectric actuator and compliant mechanism combination for maximum energy efficiency". *Smart Materials and Structures*, Vol. 14, No. 6, p. 1421. doi:10.1088/0964-1726/14/6/035.

Akedo, J., Ando, A., Bar-Cohen, Y., Cardoso, V., Cochran, S., Jeong, D.Y., Johnson, S., Kimura, M., Korobova, N., Lanceros-Méndez, S., Liao, X., Lim, L.C., Luo, L., Luo, H., Lynch, C., Maurya, D., Nagata, H., Priya, S., Ribeiro, C., Ryu, J., Saigusa, Y., Shur, V., Takenaka, T., Uchino, K., Wasa, K. and Zhao, X., 2017. *Advanced Piezoelectric Materials*. Woodhead Publishing in Materials. Woodhead Publishing.

Antoniou, A., 1969. "Realization of gyrators using operational amplifiers, and their use in rc-active-network synthesis". *IEEE Proc*, Vol. 116, No. 11, pp. 1838–1850.

He, L., Zheng, W., Zhao, C. and Wu, C., 2019. "Piezoelectric shunt stiffness in rhombic piezoelectric stack transducer with hybrid negative-impedance shunts: Theoretical modeling and stability analysis". *Sensors*, Vol. 15, No. 19, p. 3387. doi:https://doi.org/10.3390/s19153387.

Lesieutre, G., 1998. "Vibration damping and control using shunted piezoelectric materials". *Shock and Vibration Digest*, Vol. 30, No. 2, pp. 181–190.

Liu, Y. and Wang, L., 2023. "A robust-based configuration design method of piezoelectric materials for mechanical load identification considering structural vibration suppression". *Computer Methods in Applied Mechanics and Engineering*, Vol. 410, No. 17, p. 115998. ISSN 0045-7825. doi:https://doi.org/10.1016/j.cma.2023.115998.

Machado, M.R., Fabro, A.T. and Moura, B.B., 2020. "Spectral element approach for flexural waves control in smart material beam with single and multiple resonant impedance shunt circuit". *J. Comput. Nonlinear Dynam*, Vol. 15, No. 12, p. 121003.

Machado, M.R., Moura, B.B., Dey, S. and Mukhopadhyay, T., 2022. "Bandgap manipulation of single and multi-frequency smart metastructures with random impedance disorder". *Smart Materials and Structures*, Vol. 31, No. 10, p. 105020.

Mahapatra, S.D., Mohapatra, P.C., Aria, A.I., Christie, G., Mishra, Y.K., Hofmann, S. and Thakur, V.K., 2021. "Piezoelectric materials for energy harvesting and sensing applications: Roadmap for future smart materials". *Advanced Science*, Vol. 8, No. 17, p. 2100864. doi:https://doi.org/10.1002/advs.202100864.

Molter, A., dos Santos, F.L. and Brum, L.J., 2019. "An optimality criteria-based method for the simultaneous optimization of the structural design and placement of piezoelectric actuators". *Structural and Multidisciplinary Optimization*.

Moura, B.B., Machado, M.R., Mukhopadhyay, T. and Dey, S., 2022. "Dynamic and wave propagation analysis of periodic smart beams coupled with resonant shunt circuits: passive property modulation". *Eur. Phys. J. Spec. Top*, Vol. 231, pp. 1415–1431.

Niederberger, D. and Morari, M., 2006. "An autonomous shunt circuit for vibration damping". *Smart Materials and Structures*, Vol. 15, No. 2, p. 359.

Pan, H.H. and Guan, J.C., 2022. "Stress and strain behavior monitoring of concrete through electromechanical impedance using piezoelectric cement sensor and pzt sensor". *Construction and Building Materials*, Vol. 324, p. 126685. doi: https://doi.org/10.1016/j.conbuildmat.2022.126685.

Riodan, R.H.S., 1967. "Simulated inductors using differential amplifiers". *Electron. Lett*, Vol. 3, No. 2, pp. 50–51.

Rui, Q., Liang, W., Jiamei, J., Lushen, g.Y., Dandan, Z. and Yuning, G., 2023. "Enhanced semi-active piezoelectric vibration control method with shunt circuit by energy dissipations switching". *Mechanical Systems and Signal Processing*, Vol. 201, No. 19, p. 110671. doi:https://doi.org/10.1016/j.ymssp.2023.110671.

Tellegen, B.D.H., 1948. "The gyrator, a new electric network element". *Philips Res. Rep*, Vol. 3, pp. 81–101.

Viana, F.A. and Junior, V.S., 2006. "Multimodal vibration damping through piezoelectric patches and optimal resonant shunt circuits". *Journal of the Brazilian Society of Mechanical Sciences and Engineering*, Vol. 15, No. 2, p. 359.

Wang, L., Zhao, Y., Liu, J. and Zhou, Z., 2023. "Uncertainty-oriented optimal pid control design framework for piezoelectric structures based on subinterval dimension-wise method (sdwm) and non-probabilistic time-dependent reliability (ntdr) analysis". *Journal of Sound and Vibration*, Vol. 549, No. 19, p. 117588. doi: https://doi.org/10.1016/j.jsv.2023.117588.

Yamada, K., Matsuhisa, H. and Utsuno, H., 2010. "Optimum tuning of series and parallel lr circuits for passive vibration suppression using piezoelectric elements". *Journal of Sound and Vibration*, Vol. 329, No. 24, pp. 5036–5057.

Yamada, K., Matsuhisa, H. and Utsuno, H., 2013. "Enhancement of efficient of vibration suppression using piezoelectric elements and lr circuit by amplification electrical resonance". *Journal of Sound and Vibration*, Vol. 333, pp. 1281–1301.

Zambolini-Vicente, B.G.G.L., Lima, A.M.G.d. and Finzi Neto, R.M., 2017. "Experimental evaluation of synthetic inductors applied in passive shunt circuits to vibration mitigation". *Revista Interdisciplinar de Pesquisa em Engenharia*, Vol. 2, No. 13, pp. 131–141.

Zhu, X., Chen, Z. and Jiao, Y., 2018. "Optimizations of distributed dynamic vibration absorbers for suppressing vibrations in plates". *Journal of Low Frequency Noise Vibration and Active Control*, Vol. 37, No. 4, p. 1188 – 1200. doi: 10.1177/1461348418794563. Cited by: 17; All Open Access, Gold Open Access.

6. RESPONSIBILITY NOTICE

The authors are solely responsible for the printed material included in this paper.